Spin disorder in maghemite nanoparticles investigated using polarized neutrons and nuclear resonant scattering

2016 J. Phys.: Conf. Ser. 711 012002

(http://iopscience.iop.org/1742-6596/711/1/012002)

Spin disorder in maghemite nanoparticles investigated using polarized neutrons and nuclear resonant scattering

M. Herlitschke[1,2,3], S. Disch[4,5], I. Sergueev[1], K. Schlage[1], E. Wetterskog[6], L. Bergström[7], R. P. Hermann[2,3,8]

[1] FS-PE, Deutsches Elektronen-Synchrotron, 22607 Hamburg (Germany)
[2] JCNS and PGI, JARA-FIT, Forschungszentrum Jülich GmbH, 52425 Jülich (Germany)
[3] Faculté des Sciences, Université de Liège, 4000 Liège (Belgium)
[4] Department Chemie, Universität zu Köln, 50939 Köln (Germany)
[5] Institut Laue-Langevin, 38042 Grenoble (France)
[6] Department of Engineering Sciences, Angström Laboratory, 75121 Uppsala (Sweden)
[7] Department of Materials and Environmental Chemistry, Stockholm University, 10691 Stockholm (Sweden)
[8] Materials Science and Technology Division, Oak Ridge National Laboratory, 37831 Oak Ridge, Tennessee (USA)

E-mail: marcus.herlitschke@desy.de, sabrina.disch@uni-koeln.de

Abstract. The manuscript reports the investigation of spin disorder in maghemite nanoparticles of different shape by a combination of polarized small-angle neutron scattering (SANSPOL) and nuclear forward scattering (NFS) techniques. Both methods are sensitive to magnetization on the nanoscale. SANSPOL allows for investigation of the particle morphology and spatial magnetization distribution and NFS extends this nanoscale information to the atomic scale, namely the orientation of the hyperfine field experienced by the iron nuclei. The studied nanospheres and nanocubes with diameters of 7.4 nm and 10.6 nm, respectively, exhibit a significant spin disorder. This effect leads to a reduction of the magnetization to 44 % and 58 % of the theoretical maghemite bulk value, observed consistently by both techniques.

1. Introduction

Magnetic nanomaterials are nowadays used in a wide range of applications, *e.g.*, spintronics, cell labelling for magnetic separation, magnetic resonance imaging contrast enhancement, drug delivery or magnetic hyperthermia[1, 2, 3]. A large number of these applications rely on magnetic interparticle interactions or on intraparticle magnetism, motivating further investigation of the intraparticle spin structure. The overall magnetic moment of small particles is typically lower than the bulk value[4, 5], a phenomenon largely attributed to surface effects[6, 7, 8] with a surface layer often thought of as a spin glass[9, 10, 11]. Whereas a core-shell model of spin canting is often used for simplicity and conveniently reducing the number of free parameters in modelling[12, 13], recent studies of the spatial magnetization distribution in magnetic nanoparticles suggest that spin disorder in the nanoparticle core plays a major role for the magnetization of the particle[14].

Here, we present studies of reduced magnetization and the concomitant spin disorder in iron oxide nanoparticles of different shape by application of two different techniques: Polarized

Small-Angle Neutron Scattering (SANSPOL) and Nuclear Forward Scattering (NFS). These methods give access to different information, as SANSPOL is sensitive to the spatially resolved magnetization distribution and NFS is indirectly sensitive to the spin orientation of iron atoms influencing the nuclear hyperfine field in the nanomaterial. Our results indicate a significant degree of spin disorder in the studied nanoparticles, observed with both techniques, in agreement with macroscopic measurements and the literature.

2. Experimental

Particle Synthesis

Maghemite nanoparticles of spherical and cubic shape were prepared according to a thermolytic, oleic-acid-assisted synthesis route described previously [15, 16, 17]. For preparation of ^{57}Fe-enriched nanoparticles, the starting material $^{57}FeCl_3$ was prepared by heating elemental ^{57}Fe in an anhydrous Cl_2 gas stream[18]. Anhydrous Cl_2 gas was produced by oxidation of concentrated hydrochloric acid with $KMnO_4$. The evolving Cl_2 gas stream was washed from excess HCl using H_2O, dried over concentrated H_2SO_4, and subsequently passed over pieces of ^{57}Fe (0.5 g, 8.8 mmol) heated to 250°C in inert atmosphere. $^{57}FeCl_3$ (1.208 g, 7.4 mmol, 84 %) was collected as a dry, but strongly hygroscopic, shiny violet powder which turned quickly into a yellow paste when subjected to air. Mössbauer spectroscopy confirmed the high purity of the produced nanoparticles, see the supplementary data.

Morphological Characterization

Transmission electron microscopy (TEM) images were obtained using a JEOL JEM-2100 microscope equipped with a LaB_6 filament operated at 200 kV ($f = 2.7$ mm, $Cs = 1.4$ mm, $Cc = 1.8$ mm, and point resolution 2.5 Å). Small-angle X-ray Scattering (SAXS) was carried out at the B1 beamline of HASYLAB/DESY using an incident X-ray energy of 8.92 keV. The small-angle scattering was recorded using a Pilatus 300K detector set up at 0.935 and 3.635 m distances from the sample position. The data measured by dilute nanoparticle dispersions in toluene (7 mg/ml) were averaged circularly and analyzed according to spherical particle form factors.

SANSPOL

Polarized Small-angle Neutron Scattering (SANSPOL) data was collected at the D33 instrument at the Institut Laue-Langevin, using 6 Å neutron wavelength and 5.3 m detector and collimation distance. Dilute dispersions (7 mg/ml) of nanospheres and nanocubes in toluene (deuterated by 80 %) were measured with a polarized incident neutron beam ($P = 0.826$) in a horizontally applied magnetic field of 1 T. Data correction to the scattering background of the pure solvent and normalization to absolute intensities were carried out using the SANS data reduction software GRASansP[19]. The purely nuclear (I_N) as well as the nuclear-magnetic (I(+) and I(-)) scattering cross sections were radially integrated in 10 ° sectors oriented parallel and perpendicular to the applied magnetic field, respectively.

NFS

Nuclear Forward Scattering (NFS) measurements were performed at beam line P01 of the large scale facility PETRA III. The nanoparticles were dispersed in toluene with a concentration of $\approx$ 14 mg/ml and put into a sample holder with 8 mm thickness. The sample was inserted in the pre-cooled cryostat, in order to obtain a rapid freezing of toluene, with the field-cooled (FC) procedure and a magnetic field of 0.7 T, reaching a sample temperature of $15 - 30$ K. The FC procedure reproduces similar conditions as for the SANSPOL measurements, because the particle easy axis will align parallel to the field at room temperature and the solution will freeze

in this state on passing the solidification point of toluene. The magnetic field was sequentially applied, through rotation of the magnet, along the x, y and z direction.

3. Theory

Nuclear Forward Scattering - Fitting Model

The spin canting can be studied in Mössbauer spectroscopy by analyzing the ratio of different lines in a spectrum, which gives an average direction of the local magnetic field. Here, we introduce a similar approach to investigate the nuclear-forward-scattering time spectra, where an average spin direction can be obtained without a preliminary introduced model. The amplitude of the scattering consists of several components defined by the principal axis system of the polarized synchrotron beam. The ratio of these components describes the relative orientation of the hyperfine field to these axes. As shown in this section, the projections on x, y and z are useful and enable to continuously interpolate between spins randomly oriented in 3D and spins fully aligned in a specific direction.

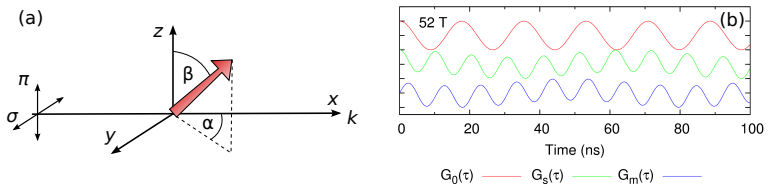

Figure 1. (a) Sketch of the coordinate system. The red arrow indicates the direction of an arbitrary hyperfine field, determined by the angles α and β. The propagation vector of the beam, k, is along the x direction, σ and π polarizations are along y and z, respectively. (b) Schematic representation of the G-terms, described in the text, for an iron nucleus in a hyperfine field of 52 T.

The NFS *amplitudes* for linear-polarised incoming radiation in case of a static hyperfine magnetic field and thin samples can be derived from Ref. [20, 21]. These amplitudes, for the chosen coordinate system depicted in figure 1, are:

$$A_{\sigma\sigma} = \frac{1}{2}(G_0(\tau) + G_s(\tau) + [G_0(\tau) - G_s(\tau)]\cos 2\beta) \tag{1}$$

$$A_{\sigma\pi} = G_m(\tau)\cos\alpha\sin\beta - (G_0(\tau) - G_s(\tau))\frac{1}{2}\sin 2\beta\sin\alpha \tag{2}$$

$$G_0(\tau) = \cos\frac{\tau(\omega_e - \omega_g)}{2} \tag{3}$$

$$G_s(\tau) = \frac{3}{4}\cos\frac{\tau(3\omega_e - \omega_g)}{2} + \frac{1}{4}\cos\frac{\tau(\omega_e + \omega_g)}{2} \tag{4}$$

$$G_m(\tau) = \frac{3}{4}\sin\frac{\tau(3\omega_e - \omega_g)}{2} + \frac{1}{4}\sin\frac{\tau(\omega_e + \omega_g)}{2}, \tag{5}$$

where $A_{\sigma\sigma}$ is the amplitude without polarization change and $A_{\sigma\pi}$ is the amplitude with polarization change. The constants $\omega_e = B \cdot 4.96\,(\mu\mathrm{s}\cdot\mathrm{T})^{-1}$ and $\omega_g = -B \cdot 8.68\,(\mu\mathrm{s}\cdot\mathrm{T})^{-1}$ are the Larmor frequencies in the field B/μ_0 of the ^{57}Fe 14.4 keV excited and ground state, respectively. The perturbation factors $G(\tau)$, depicted in figure 1, describe the nuclear transitions. $G_0(\tau)$ corresponds to transitions with magnetic quantum number $M = 0$, and the $G_s(\tau)$ and $G_m(\tau)$ correspond to $M = \pm 1$. Transformed into the frequency domain, G_0 reproduces the lines 2 and 5 of a Mössbauer spectrum, and G_s and G_m reproduce the lines $1, 3, 4$ and 6.

The given scattering amplitudes enable the calculation of a time spectrum for any configuration of the hyperfine field, by going from the amplitudes to the intensities with an

Table 1. Selected hyperfine field orientations and the resulting scattering amplitudes. The x^+ indicates nuclei with hyperfine field in the beam propagation direction, $x^\pm$ indicates an equal number of nuclei with hyperfine fields parallel and antiparallel to the beam propagation direction.

	$A_{\sigma\sigma}$	$A_{\sigma\pi}$
$H_{hf} \parallel z$	G_0	0
$H_{hf} \parallel y$	G_s	0
$H_{hf} \parallel x^+$	G_s	G_m
$H_{hf} \parallel x^\pm$	G_s	0
3D powder	$\frac{1}{3}(G_0 + 2G_s)$	0

additional exponential decay. Several orientations and the resulting amplitudes are compared in table 1. For example, assuming a hyperfine field along z ($\beta = 0$ and $\alpha =$ arbitrary), leads to $A_{\sigma\sigma} = G_0$ and $A_{\sigma\pi} = 0$. If several directions of the hyperfine field exist, the total amplitude will be the sum of partial amplitudes.

When this description of NFS is applied to the scattering signal of the nanoparticles, different aspects have to be considered: the spins in the maghemite particles order ferrimagnetically within one particle, forming a macro moment. But on the atomic length scale, spins are not perfectly in the ferrimagnetic order but rather canted [5, 14, 11]. The corresponding hyperfine field experienced by the ^{57}Fe nucleus is anti-parallel to the spin due to the Fermi contact term. An applied magnetic field parallel to the z axis, see figure 1, leads to orientation of the particle moment and the canted spins form a distribution that is symmetric around the applied field direction. This symmetry around the field is not a unique behaviour of the canting effect but rather a general observation, because the only present preferential direction in the sample is the field direction. Thus, the orthogonal plane behaves powder-like and all directions are energetically equal.

In order to describe this distribution of spins, a function $f(\beta)$ is assumed with $\int_0^\pi f(\beta)\sin\beta\, d\beta = 1$, expressing the hyperfine field orientation density in a particular direction, with respect to the z axis. Introducing this function $f(\beta)$ in the amplitudes $A_{\sigma\sigma}$ and $A_{\sigma\pi}$ and performing a volume integration leads to the averaged amplitudes $A^{(z)}_{\sigma\sigma}$ and $A^{(z)}_{\sigma\pi}$. The resulting G_0 and G_s terms can be separated:

$$\begin{aligned} A^{(z)}_{\sigma\sigma} =& \frac{1}{4\pi}\int_0^{2\pi} d\alpha \int_0^{\pi} d\beta \quad f(\beta)\sin\beta\; A_{\sigma\sigma} \\ =& G_0 \int_0^{\pi} d\beta \quad f(\beta)\sin\beta\; \frac{1}{4}(1+\cos 2\beta) \\ &+ G_s \int_0^{\pi} d\beta \quad f(\beta)\sin\beta\; \frac{1}{4}(1-\cos 2\beta) \\ =& G_0 a^{(z)} + G_s b^{(z)} \propto G_0 + G_s c^{(z)}_{\sigma\sigma}. \end{aligned} \tag{6}$$

The obtained parameters $a^{(z)}$ and $b^{(z)}$ are constant, since the integration over β can be performed for a given $f(\beta)$ leading to a scalar. The constant $c^{(z)}_{\sigma\sigma}$ gives a quantitative description of the function $f(\beta)$, but more than one function $f(\beta)$ can lead to the same $c^{(z)}_{\sigma\sigma}$ and thus to the same scattering signal. The same procedure can be performed for the amplitude $A_{\sigma\pi}$ leading to $A^{(z)}_{\sigma\pi} = 0$, due to vanishing integration over α. Comparing these amplitudes with table 1, one can conclude that $c^{(z)}_{\sigma\sigma} = 2$ describes the 3D random case and $c^{(z)}_{\sigma\sigma} = 0$ describes the perfect alignment parallel to z. More generally, a sum of configurations from table 1 can be used in

order to describe the scattering for an arbitrary function $f(\beta)$, since only the G_0 and G_s terms are necessary in order to represent $f(\beta)$.

The same procedure can be applied for other quantization axes, *e.g.*, in case of an applied magnetic field along y or x. For sake of simplicity, the coordinate system should be changed in such way that the polar angle θ is always between the hyperfine field and the externally applied magnetic field. Consequently, the amplitudes need to be transformed to the new coordinate system. The integration over α can always be performed due to the rotation symmetry around the applied magnetic field and a description of the function $f(\beta)$ will be obtained for the new coordinate system. For the case of a magnetic field along y one obtains:

$$A_{\sigma\sigma}^{(y)} \propto c_{\sigma\sigma}^{(y)} \frac{1}{2}(G_0 + G_s) + G_s \tag{7}$$

$$A_{\sigma\pi}^{(y)} = 0. \tag{8}$$

This case is different from the former in that a complete alignment of the hyperfine field along the y axis results in $A_{\sigma\sigma}^{(y)} \propto G_s$, whereas the 3D random alignment is again $A_{\sigma\sigma}^{(y)} \propto G_0 + 2G_s$. The $\frac{1}{2}(G_0 + G_s)$ term represents a 2D alignment orthogonal to the field.

The case of a magnetic field parallel to the beam and thus along x is the most complex one, because the scattering process is sensitive to the relative amount of hyperfine fields parallel and anti-parallel to the applied field. The amplitudes are:

$$A_{\sigma\sigma}^{(x)} \propto c_{\sigma\sigma}^{(x)} \frac{1}{2}(G_0 + G_s) + G_s \tag{9}$$

$$A_{\sigma\pi}^{(x)} \propto c_{\sigma\pi}^{(x)} G_m. \tag{10}$$

A complete alignment of all hyperfine fields either parallel or anti-parallel to the beam correspond to $c_{\sigma\sigma}^{(x)} = 0$ and $c_{\sigma\pi}^{(x)} = 1$. In case the observed hyperfine fields are parallel and anti-parallel to the beam with equal amount, the constants will be $c_{\sigma\sigma}^{(x)} = 0$ and $c_{\sigma\pi}^{(x)} = 0$. The 3D random case is represented with $c_{\sigma\sigma}^{(x)} = 2$ and $c_{\sigma\pi}^{(x)} = 0$. As a remark, the amplitudes can be scaled by a constant factor in the analysis, as done before, but both amplitudes have to be scaled in the same way in order to not influence the resulting fit with the scaling.

Summarizing, the constants $c_{\sigma\sigma}^{(x,y,z)}$ were always defined such that a value of zero corresponds to a complete alignment of all hyperfine fields and thus of all spins. A value of $c_{\sigma\sigma}^{(x,y,z)} = 2$ correspond always to the 3D random case for all three field directions. In contrast, $c_{\sigma\pi}^{(x)}$ is defined such that a value of zero corresponds to an equal number of the hyperfine fields parallel and anti-parallel to the beam and a value of one denotes the case of either complete parallel or anti-parallel alignment.

4. Results and Discussion

^{57}Fe-enriched nanoparticles

Maghemite (γ-Fe_2O_3) nanoparticles of spherical and cubic shape, enriched with ^{57}Fe, were prepared according to previously published synthesis routes [15, 16, 17]. Small-angle X-ray Scattering (not shown) confirms the narrow particle size distribution inferred by TEM analysis, yielding a spherical particle radius of 3.68(1) nm with a lognormal size distribution of $\sigma_{log} = 0.057(5)$. For the nanocubes, approximated with a spherical particle form factor due to their orientation distribution in dispersion, a particle radius of 5.28(1) nm is obtained, along with a slightly larger size distribution of $\sigma_{log} = 0.070(1)$ resulting from the nonspherical shape of the particles.

The purely nuclear SANS scattering cross section (I_N) was refined according to a core-shell particle form factor, reflecting the iron oxide particle core and an oleic acid ligand shell covering

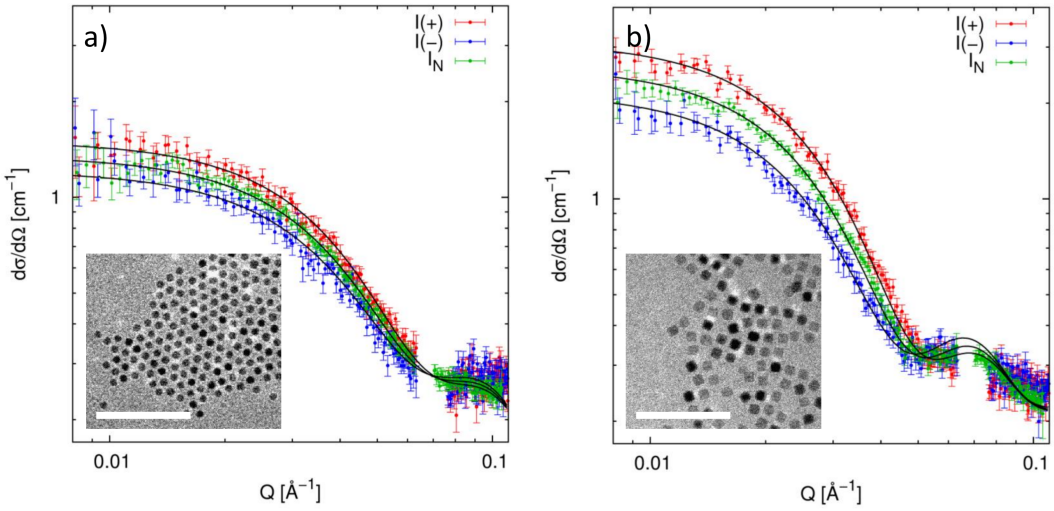

Figure 2. SANSPOL by iron oxide a) nanospheres and b) nanocubes. Purely nuclear (I_N) and nuclear-magnetic ($I(+)$, $I(-)$) cross sections, obtained from radial integration in 10 ° sectors oriented parallel and perpendicular to the applied magnetic field, are presented including refinements of the core-shell nanoparticle morphology. Missing data points are due to the gap between the two detectors at D33 (ILL). Insets: respective TEM images (scale bars: 100 nm)

the particle surface. The ligand shell thickness was determined as 1.5(1) nm and 2.0(1) nm for the spheres and cubes, respectively, in reasonable agreement with the maximum oleic acid ligand shell thickness of up to 2.1 nm. Moreover, quantitative analysis of the SANS cross sections shown in figure 2 additionally enables determination of the γ-$^{57}Fe_2O_3$ scattering length density of $4.96(5) \cdot 10^{-6}$ Å^{-2} which, consistently for both samples, indicates a degree of ^{57}Fe enrichment of 65(5) %.

Polarized Small-Angle Neutron Scattering

Polarized SANS (SANSPOL) was carried out in order to determine the magnetic morphology of the samples via the magnetic form factor. For a dilute system of non-interacting particles aligned in an external field, the nuclear and magnetic scattering amplitudes F_N and F_M interfere according to

$$I(\pm)_{Q,\alpha} = F_N^2(Q) + [F_M^2(Q) \mp 2\varrho^{\pm} F_N(Q) F_M(Q)] \sin^2 \alpha \tag{11}$$

$$I(+)_{Q,\alpha} - I(-)_{Q,\alpha} = -2(\varrho^+ + \varrho^-) F_N(Q) F_M(Q) \sin^2 \alpha \tag{12}$$

where α is the azimuthal angle between the scattering vector Q and the applied magnetic field direction, and $\varrho^+ = P, \varrho^- = P\epsilon$ with $P = 0.826$ being the degree of polarization of the incident neutrons and $\epsilon = 0.99$ the flipper efficiency. The polarized SANS cross sections $I(+)$ and $I(-)$ for the nanospheres and nanocubes are presented in figure 2 along with refinements according to equation (11). Refinements of the nuclear-magnetic cross term according to equation (12) converged to the same results, confirming self-consistency of the model.

Whereas previous studies on very similar nanoparticles revealed a small degree of surface spin canting along with a significantly reduced magnetization in the entire nanoparticles [14], refinements of the magnetic form factor of the ^{57}Fe-enriched nanoparticles consistently converge to a magnetic particle radius equal to the nuclear particle radius, irrespective of the starting model of either a core-shell magnetic particle or a particle with smoothly decreasing magnetization towards the surface. Hence, our analysis suggests a homogeneous magnetization

distribution with spin canting throughout the entire particle without any significant degree of enhanced spin disorder close to the particle surface in either sample of the ^{57}Fe-enriched nanoparticles. Quantitative analysis of the magnetic scattering length density yields an average magnetization of 0.55(2) and 0.72(2) μ_B per iron atom for the spheres and cubes, respectively, *i.e.* significantly lower than the theoretical spin-only bulk maghemite moment of 1.25 μ_B (0 K). The room temperature maghemite moment can only be estimated, as the pure bulk material is not stable. However, the value should be close to the 0 K value, as, with $T/T_C \sim 0.3$ ($T_C \sim 900$ K[22]), the room temperature measurement is far away from the magnetic transition. Further, most theoretical models lead to values close to 1.25 μ_B, *e.g.* mean-field theory gives 1.2 μ_B and Bloch's law value is between 1.0 μ_B ($\sim T^{3/2}$ for ferromagnet) and 1.2μ_B ($\sim T^3$ for antiferromagnet)[23].

For the nanocubes, the determined magnetization is in good agreement with our earlier study on similar, but non-enriched, nanocubes of comparable particle size [14]. The smaller magnetization determined for the nanospheres is in excellent agreement with the magnetization of 0.50(5) μ_B per iron atom determined by macroscopic magnetization measurements (not shown). Our results are further in general agreement with reports on the particle-size-dependent magnetization [10, 24].

Nuclear Forward Scattering

The nuclear forward scattering data with different directions of magnetic fields are depicted in figure 3. In the data analysis, each of both crystallographic iron sites is associated with two

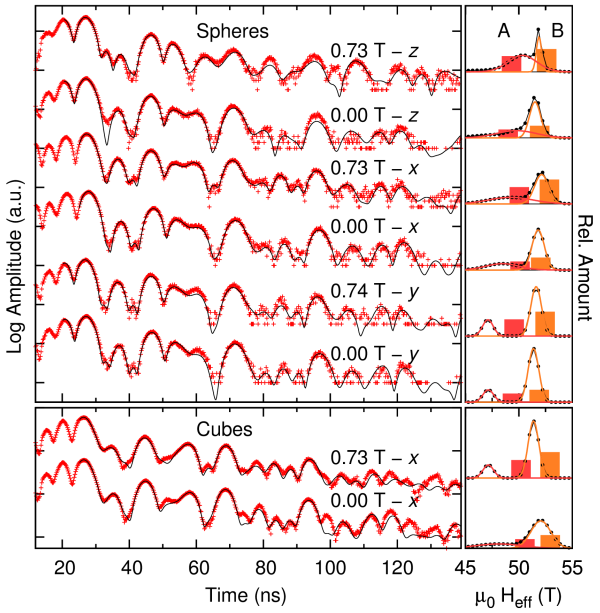

Figure 3. Adjusted NFS data on nanospheres with the indicated applied magnetic fields and a temperature of 15-30 K, depicted in logarithmic scale (left). The data were recorded at P01 with a magnetic field applied in the vertical (z) direction, horizontal direction (y), and along the beam (x). The parallel effective fields at the nuclei of A and B site (boxes) and the corresponding field distributions (Gaussian functions) are depicted for the A site in red and the B site in orange (right).

components (magnetic field along z and y) or three components (magnetic field along x). These components correspond to the relative spin orientation parallel or orthogonal to the external

magnetic field. Thus, the orientation of arbitrary spins can be described with the ratio between these components, as outlined in section 3. In contrast to the introduced projection model, the hyperfine fields of the parallel and orthogonal components are not restricted to the same value. The data fitting was performed utilizing the MOTIF code[25] with fixed values of isomer shift and quadrupole interaction, taken from Mössbauer spectral results (see the supplementary data) and in agreement with literature[22, 26].

The analysis revealed that the perpendicular components of both sites are not well described with only one dedicated hyperfine field per site. Instead a Gaussian distribution of hyperfine fields is needed. One Gaussian distribution per perpendicular component was introduced, whereas the position and the width of the Gaussian are freely adjustable. The discrepancy of the fit at latter times in all spectra is probably attributed to small contributions of superparamagnetic relaxation, neglected in the analysis. Other free parameters in the adjustment are the sample thickness, an overall scaling factor, a zero shift of the measured signal, and an additional line broadening, assumed to be equal for all components.

The NFS intensities differ somewhat for different directions of the magnetic field, even for 0 T measurements. This observation is explained by different effects: first, the sample was frozen in the FC procedure leading to an alignment of the easy-axis of the nanoparticles along the field direction and thus to a preferred orientation in different directions for the individual measurements. Second, the temperatures are not exactly the same leading to slightly different hyperfine field values and also to slightly different hyperfine field distributions. For example, the temperature change between 15 and 30 K changes the hyperfine field by up to 1 T. Third, the sample thickness can slightly change between the freezing steps due to the remounting of the liquid sample, which strongly influences the time pattern.

Table 2. Adjusted parameters of the A and B site obtained from analysis of the NFS data leading to the constants $c_{\sigma\sigma}$ and $c_{\sigma\pi}$ for different magnetic fields H in direction x, y or z. The relative amount of the parallel components $\xi_{\parallel} = (A_{\parallel} + B_{\parallel})$ is related to these constants, as described in the theory part.

	$\mu_0 H$ (T)	$c_{\sigma\sigma}$	$c_{\sigma\pi}$	$\frac{\xi_{\parallel}}{\xi_{\parallel}+\xi_{\perp}}$
Spheres	0.73 - z	1.16(1)	-	0.46(1)
	0.00 - z	2.24(3)	-	0.31(2)
	0.73 - x	0.93(8)	0.20(4)	0.52(5)
	0.00 - x	1.61(24)	0.11(3)	0.38(6)
	0.73 - y	0.96(2)	-	0.51(1)
	0.00 - y	1.87(4)	-	0.35(1)
Cubes	0.73 - x	0.80(6)	0.28(4)	0.55(4)
	0.00 - x	1.53(16)	0.21(4)	0.39(4)

The observed differences in the spectra with different field directions seem more distinct than those in the same directions with and without applied field. However, the analysis reveals the opposite. The 0 T measurements correspond to very similar physical parameters and the application of a magnetic field changes the hyperfine field orientation and thus the ratio of aligned spins, depicted in table 2. The alignment of the spins leads to a decrease of the $c_{\sigma\sigma}$ parameter and an increase of the relative fraction of parallel spins. The value $\xi_{\parallel}/(\xi_{\parallel}+\xi_{\perp}) = 1/3$, with $\xi_{\parallel}$ the amount of the components with parallel hyperfine field and $\xi_{\perp}$ the amount of the components with perpendicular hyperfine field, is expected for zero field measurements, because it describes the complete 3D random case. The observed discrepancies between the obtained values at 0 T and the expected ratio of 1/3 is probably reasoned by preferred orientation of

the particles due to the freezing process, remanent magnetization and time dependent macro moment reorientation, as described by Sharrock's formula[27].

In an applied field of 0.73 T, the atomic moments of the nanospheres align up to 50 %, whereas the variance is quite large with $46 - 52$ %. This result is similar to magnetometry data exhibiting only a magnetization of $\sim 0.5\,\mu_B$ in contrast to the theoretically expected $1.25\,\mu_B$ for bulk maghemite (0 K). But, $\xi_{\parallel}/(\xi_{\parallel}+\xi_{\perp})$ gives only the fraction of parallel *plus* anti-parallel spins and does not indicate the relative ratio between them. This ratio between parallel and anti-parallel spins will influence the total magnetic moment significantly, as magnetometry measures the macroscopic sum of all atomic moments. The hyperfine fields and thus the spins within the larger nanocubes exhibit a stronger orientation with applied magnetic field of about 55 % as compared to the nanospheres.

The $c_{\sigma\pi}$ constant is the most difficult and the most unstable parameter to adjust. Furthermore, this component depends strongly on the applied model and can change drastically by changing the degrees of freedom in the adjustment. The strong change is probably reasoned by the frequency of the G_m term being equal to the frequency of the G_s term and thus allowing the G_m term to compensate discrepancies in the adjustment. However, the main trend of an increasing $c_{\sigma\pi}$ with application of a magnetic field and thus a non-equal orientation of spins parallel and anti-parallel along the beam is obvious. Again, comparing the $c_{\sigma\pi}$ parameter of nanospheres and nanocubes, the cubes seem to be more aligned.

In a first, rough approximation, the canting of the spins observed with NFS can be compared to the reduced magnetization obtained by SANSPOL. The canting determined by NFS relates to $0.62(6)\,\mu_B$ and $0.69(5)\,\mu_B$ for the nanospheres and nanocubes, respectively, as the magnetization is only the parallel fraction of the magnetic moments in the sample. This result is similar to the moments observed with SANSPOL, however, the nanospheres magnetic moment determined with NFS seems to be higher than observed with SANSPOL. Such difference is reasonable due to the temperature dependence of the canting[28, 29], expected to decrease the room temperature magnetization by a few percent. But this effect was not observed for the cubes, whereas the large error bars of NFS results may prohibit this observation. Another explanation for the larger moment of the nanospheres is found in $c_{\sigma\pi}$. The smaller $c_{\sigma\pi}$ of the nanospheres indicates that the relative ratio between parallel and anti-parallel spins is less pronounced, as compared to the nanocubes. Thus, a further reduction of the nanosphere moment due to compensating parallel and anti-parallel spins is possible, not considered in the rough approximation of the magnetic moments.

Summarizing, both methods, namely SANSPOL and NFS, confirm the reduced magnetization commonly observed in maghemite nanoparticles in agreement with literature and macroscopic measurements. The spatial sensitivity of the SANSPOL technique reveals a homogeneous distribution of the reduced particle magnetization, corresponding to homogeneously distributed spin disorder, with negligible effects of the particle surface. The SANSPOL results are similar to the NFS analysis, indicating a random orientation of about half of the atomic moments. Thus, roughly the half of the iron atoms are not in the perfect ferrimagnetic order.

5. Acknowledgements

SD acknowledges funding by the 7th European Community Framework Programme (PIEF-GA-2011-298918) and financial support from the Fonds der Chemischen Industrie. RPH acknowledges the Helmholtz Association of German Research Centers for funding VH NG-407 "Lattice dynamics in emerging functional materials" and support from the Materials Sciences and Engineering Division, Office of Basic Energy Sciences, U.S. Department of Energy. LB and EW acknowledge the Swedish Research Council (VR) for funding. Portions of this research were carried out at the light source PETRA III at DESY, a member of the Helmholtz Association (HGF). We would like to thank H.-C. Wille for assistance in using beamline P01.

References

[1] Kozissnik B and Dobson J 2013 *MRS Bulletin* **38** 927–932 URL http://dx.doi.org/10.1557/mrs.2013.257
[2] Pankhurst Q A, Connolly J, Jones S K and Dobson J 2003 *Journal of Physics D: Applied Physics* **36** R167 URL http://stacks.iop.org/0022-3727/36/i=13/a=201
[3] Bader S D 2006 *Rev. Mod. Phys.* **78** 1–15 URL http://link.aps.org/doi/10.1103/RevModPhys.78.1
[4] Morrish A and Sawatzky G 1971 *Proc. Int. Conf. Ferrites, University of Tokyo Press* 144
[5] Batis-Landoulsi H and Vergnon P 1983 *J Mater Sci* **18** 3399 ISSN 0022-2461 URL http://dx.doi.org/10.1007/BF00544166
[6] Coey J M D 1971 *Phys. Rev. Lett.* **27** 1140–1142 URL http://link.aps.org/doi/10.1103/PhysRevLett.27.1140
[7] Tronc E, Prené P, Jolivet J, Dormann J and Grenèche J 1998 *Hyperfine Interact* **112** 97–100 ISSN 0304-3843 URL http://dx.doi.org/10.1023/A%3A1011092712136
[8] Mørup S 2003 *Journal of Magnetism and Magnetic Materials* **266** 110–118 ISSN 0304-8853
[9] Kodama R 1999 *Journal of Magnetism and Magnetic Materials* **200** 359–372 ISSN 0304-8853 URL http://www.sciencedirect.com/science/article/pii/S0304885399003479
[10] Morales M P, Veintemillas-Verdaguer S, Montero M I, Serna C J, Roig A, Casas L, Martinez B and Sandiumenge F 1999 *Chem. Mater.* **11** 3058–3064 ISSN 0897-4756 URL http://dx.doi.org/10.1021/cm991018f
[11] Restrepo J, Labaye Y and Greneche J 2006 *Physica B: Condensed Matter* **384** 221–223 ISSN 0921-4526 URL http://www.sciencedirect.com/science/article/pii/S0921452606011434
[12] Krycka K L, Booth R A, Hogg C R, Ijiri Y, Borchers J A, Chen W C, Watson S M, Laver M, Gentile T R, Dedon L R, Harris S, Rhyne J J and Majetich S A 2010 *Phys. Rev. Lett.* **104** 207203 URL http://link.aps.org/doi/10.1103/PhysRevLett.104.207203
[13] Tronc E, Ezzir A and Cherkaoui R, Chanéac C, Noguès M, Kachkachi H, Fiorani D, Testa A M, Grenèche J M and Jolivet J P 2000 *Journal of Magnetism and Magnetic Materials* **221** 63–79 ISSN 0304-8853 URL http://www.sciencedirect.com/science/article/pii/S0304885300003693
[14] Disch S, Wetterskog E, Hermann R P, Wiedenmann A, Vainio U, Salazar-Alvarez G, Bergström L and Bückel T 2012 *New Journal of Physics* **14** 013025 URL http://stacks.iop.org/1367-2630/14/i=1/a=013025
[15] Park J, An K, Hwang Y, Park J G, Noh H J, Kim J Y, Park J H, Hwang N M and Hyeon T 2004 *Nat Mater* **3** 891 ISSN 1476-1122 URL http://dx.doi.org/10.1038/nmat1251
[16] Ahniyaz A, Sakamoto Y and Bergström L 2007 *Proceedings of the National Academy of Sciences* **104** 17570–17574 URL http://www.pnas.org/content/104/45/17570.abstract
[17] Wetterskog E, Agthe M, Mayence A, Grins J, Wang D, Rana S, Ahniyaz A, Salazar-Alvarez G and Bergström L 2014 *Science and Technology of Advanced Materials* **15** 055010– ISSN 1468-6996 URL http://stacks.iop.org/1468-6996/15/i=5/a=055010
[18] Tarr B R, Booth H S and Dolance A 1950 *Inorganic Syntheses* (John Wiley and Sons, Inc.) pp 191–194 URL http://dx.doi.org/10.1002/9780470132340.ch51
[19] Dewhurst C 2008 Graphical reduction and analysis sans program for matlab URL https://www.ill.eu/instruments-support/instruments-groups/groups/lss/grasp
[20] Dattagupta S 1981 *Hyperfine Interact* **11** 77–126 ISSN 0304-3843 URL http://dx.doi.org/10.1007/BF01026470
[21] Shvyd'ko Y V 1999 *Hyperfine Interact* **123-124** 275–299 ISSN 0304-3843 URL http://dx.doi.org/10.1023/A%3A1017015721916
[22] Long G J 1987 *Mössbauer Spectroscopy Applied to Inorganic Chemistry Volume 2* (Plenum Press)
[23] Blundell S 2001 *Magnetism in Condensed Matter* (Oxford)
[24] Millan A, Urtizberea A, Silva N, Palacio F, Amaral V, Snoeck E and Serin V 2007 *Journal of Magnetism and Magnetic Materials* **312** L5–L9 ISSN 0304-8853 URL http://www.sciencedirect.com/science/article/pii/S0304885306010717
[25] Shvyd'ko Y V 2000 *Hyperfine Interact* **125** 173–188 ISSN 0304-3843 URL http://dx.doi.org/10.1023/A%3A1012633620524
[26] Helgason O, Rasmussen H K and Morup S 2006 *Journal of Magnetism and Magnetic Materials* **302** 413–420 ISSN 0304-8853 URL http://www.sciencedirect.com/science/article/pii/S0304885305007973
[27] Bedanta S, Petracic O and Kleemann W 2014 *Handbook Of Magnetism Vol. 22* (in print)
[28] Zulfiqar, Rahman M, Usman M, Hasanain S, ur Rahman Z, Ullah A and Kim I 2014 **65** 1925–1929– ISSN 0374-4884 URL http://dx.doi.org/10.3938/jkps.65.1925
[29] Guivar J, Martinez A, Anaya A, Valladares L, Felix L and Dominguez A 2014 *Advances in Nanoparticles* **3** 8 URL http://www.scirp.org/journal/PaperInformation.aspx?PaperID=49326

6. Supplementary data

Mössbauer spectroscopy was measured on the enriched spheres and cubes at 10 K without applied magnetic field, see figure 4. The spectra are calibrated with respect to α-Fe. The fit model assumes two crystallographic sites and a Gauss-distributed hyperfine field. The ratio of the A and B sites are fixed to 1:1.75, in agreement with the NFS data. The obtained hyperfine parameters are given in table 3. The maghemite spectra can contain different iron-oxide impurities, likely wuestite. These impurities usually form additional peaks at the indicated energies (arrows). For the samples used in this manuscript, such impurities are not adjustable in the Mössbauer spectra.

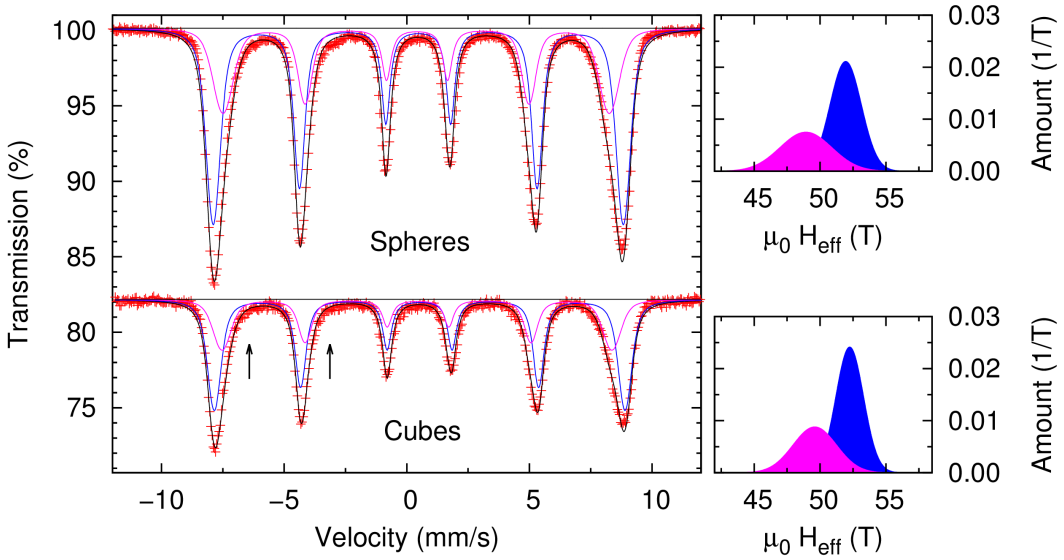

Figure 4. Adjusted Mössbauer data on nanospheres and nanocubes (left) with the corresponding hyperfine field distribution (right). The ratio of the maghemite A site (pink) and B site (blue) are fixed to 1:1.75, in agreement with the NFS data. Possible impurities, likely other oxides like wuestite, commonly lead to peaks at the indicated energies (arrows) and their presence can be excluded at the $\sim 1\,\%$ level.

Table 3. Obtained parameters from Mössbauer spectroscopy. The isomer shift δ, the quadrupole interaction ΔE_Q, the center value of the Gaussian field distribution H^{center}, and the standard deviation of the Gaussian distribution σ are given for the A and B site of both samples.

	site	δ (mm/s)	ΔE_Q (mm/s)	$\mu_0 H^{center}$ (T)	σ (T)
Spheres	A	0.40(1)	-0.03(1)	49.0(1)	2.0(3)
	B	0.48(1)	0.00(1)	52.0(1)	1.2(1)
Cubes	A	0.39(1)	-0.04(2)	49.6(1)	1.7(3)
	B	0.48(1)	0.00(1)	52.3(1)	1.1(1)